

Earthquake resistance of structural walls confined by conventional tie hoops and steel fiber reinforced concrete

Taesung Eom^{1a}, Sumin Kang^{2b} and Okkyue Kim^{*2}

¹Department of Architectural Engineering, Dankook University,
152 Jukjeon-ro, Suji-gu, Yongin-si, Gyeonggi-do, 448-701, Republic of Korea

²Department of Architectural Engineering, Chungbuk National University,
410 Seongbong-ro, Heungdeok-gu, Cheongju Chungbuk 361-763, Republic of Korea

(Received August 27, 2014, Revised September 18, 2014, Accepted September 27, 2014)

Abstract. In the present study, the seismic performance of structural walls with boundary elements confined by conventional tie hoops and steel fiber concrete (SFC) was investigated. Cyclic lateral loading tests on four wall specimens under constant axial load were performed. The primary test parameters considered were the spacing of boundary element transverse reinforcement and the use of steel fiber concrete. Test results showed that the wall specimen with boundary elements complying with ACI 318-11 21.9.6 failed at a high drift ratio of 4.5% due to concrete crushing and re-bar buckling. For the specimens where SFC was selectively used in the plastic hinge region, the spalling and crushing of concrete were substantially alleviated. However, sliding shear failure occurred at the interface of SFC and plain concrete at a moderate drift ratio of 3.0% as tensile plastic strains of longitudinal bars were accumulated during cyclic loading. The behaviors of wall specimens were examined through nonlinear section analysis adopting the stress-strain relationships of confined concrete and SFC.

Keywords: structural wall; boundary element; transverse reinforcement; steel fiber concrete; seismic performance

1. Introduction

Fig. 1(a) shows a slender reinforced concrete (RC) structural wall subjected to axial and lateral loads. Since the inelastic behavior of the wall is dominated by flexure-compression, plastic deformation concentrates on the plastic hinge region at the bottom of the wall. According to previous studies (Park *et al.* 2007, Thomsen and Wallace 1995, Wallace 1994, Wallace 1995, Wallace and Moehle 1992, Wallace and Orakcal 2002, Paulay and Priestley 1992, Sullivan 2010), the walls dominated by flexure-compression primarily fail due to concrete crushing at the boundary elements of the plastic hinge region. Therefore, in order to enhance the deformation capacity of the walls, ACI 318-11 recommends the prescriptive confinement details be provided for the boundary elements.

*Corresponding author, Professor, E-mail: okkyue@gmail.com

^aAssistant Professor, E-mail: tseom@dankook.ac.kr

^bAssistant Professor, E-mail: kangsm@chungbuk.ac.kr

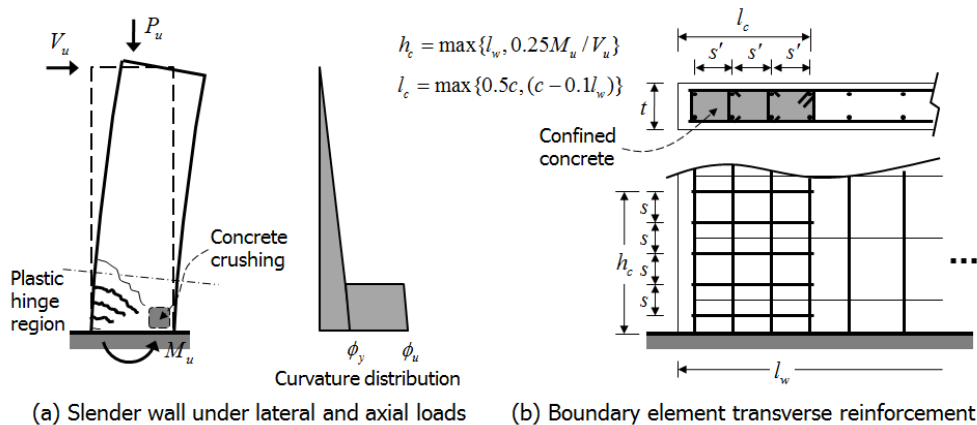


Fig. 1 Seismic design of structural walls

Fig. 1(b) illustrates the boundary element transverse reinforcement details of the special structural wall specified in ACI 318-11 21.9.6. As shown in the figure, the transverse reinforcement is used in the wall boundaries of the plastic hinge region. Basically, the amount and spacing of the transverse reinforcement are determined from the same provisions as those for columns (i.e. ACI 318-11 21.6.4), except for the vertical spacing limitation of $s \leq t/3$ (t = wall thickness). However, since the wall thickness t is relatively small when compared to the overall height of column section, the transverse reinforcement is often closely spaced in the wall boundaries. Furthermore, due to crossties used to satisfy the horizontal spacing requirement of $s' \leq 350$ mm and seismic hooks at both ends of hoops and crossties, field reinforcement work is not that simple and easy.

For steel fiber concrete (SFC), steel fibers mixed with concrete resist against tensile stress in any direction (ACI Committee 544 1988). Thus the SFC can be used along with conventional transverse reinforcement to reduce flexural and shear cracking in beams and beam-column joints. This was well verified from the previous studies on interior and exterior beam-column joints (Filiatrault *et al.* 1994, Sylvain and Jules 1995, Henager 1977, Jiuru *et al.* 1992). In addition, the ductility of SFC under compression (i.e. the post-peak descending behavior) can be improved as the steel fibers are placed in the transverse or inclined direction to the applied compression provide lateral confinement for the concrete (Craig *et al.* 1984, Chaallal *et al.* 1996). This indicates that when the SFC is used in columns and walls along with conventional transverse reinforcement, the seismic performance such as post-yield strength, deformation capacity, and energy dissipation capacity may be enhanced or at least equivalent even in the case that the strict confinement requirements of ACI 318 21.9.6 and 21.6.4 are alleviated.

In the present study, the seismic performance of structural walls with boundary elements confined by conventional tie hoops and SFC were investigated. Cyclic load tests on four wall specimens under constant axial load were performed. The spacing of transverse reinforcement and the use of SFC in the plastic hinge region were considered as the primary parameters. The earthquake resistance parameters such as load-carrying capacity, deformation capacity, energy dissipation capacity, and failure mode were investigated. In addition, the confinement effect of conventional tie hoops and SFC were examined through nonlinear section analysis.

2. Test program

2.1 Wall specimens

Fig. 2 shows the dimensions and reinforcement details of four wall specimens, RC180, RC45, SFC180, and SFC90. The test parameters are summarized in Table 1. RC180 and RC45 are the special structural wall with boundary elements confined by conventional tie hoops and crossties. On the other hand, SFC180 and SFC90 were the steel fiber reinforced concrete walls where SFC was used for the boundary elements along with tie hoops and crossties. The numbers used in the names of specimens are the spacing of the boundary element transverse reinforcement. The wall specimens were the cantilever consisting of three parts (see Fig. 2(a)): the pedestal, wall, and loading beam. The heights of the pedestal, wall, and loading beam were 650 mm, 1775 mm, and 600mm, respectively. The shear span length between the critical section and the loading point was 2000mm. The dimension of the wall cross section was 180mm x 900mm (i.e. $t = 180$ mm).

For RC180, sixteen D13 bars ($\rho = 0.0131$) were evenly distributed in two layers over the cross section as the flexure-compression reinforcement (see Fig. 2(b)). D10 bars were used at a spacing of 150mm as the horizontal shear reinforcement ($\rho_h = 0.00983$). Tie hoops and crossties of D10 bars were additionally used for the boundary element transverse reinforcement in the plastic hinge region. The tie hoops and crossties were provided over a length of 900mm from the wall bottom at a spacing of $s = 180$ mm. The boundary element extended horizontally from the compression end a distance of $l_c = 272$ mm, as shown in Fig. 2. According to ACI 318-11 21.9.6, l_c was greater than $\max\{c - 0.1l_w, 0.5c\} = \max\{148, 119\} = 148$ mm (see Fig. 1(b)), where the calculated neutral axis depth c was 238 mm. c was calculated based on the design concrete strength of 27MPa and the design steel yield strength of 400MPa, rather than the actual material strengths.

For RC45, the longitudinal and horizontal reinforcements were the same as those of RC180 (see Fig. 2(b)): sixteen D13 bars ($\rho = 0.0131$) were used for the flexure-compression reinforcement and D10 bars were used in the web at a spacing of 150 mm ($\rho_h = 0.00983$) for the shear reinforcement. However, D10 hoops and crossties were used at a spacing of $s = 45$ mm ($= 0.25t$) in the boundary elements of the plastic hinge region. The spacing of the boundary element transverse reinforcement was stricter than the requirement of ACI 318-11 21.9.6, $s \leq t/3$. Note that the spacings $s = 180$ mm and 45 mm of transverse reinforcement used in RC180 and RC45, respectively, were considered as the test parameter to investigate the effectiveness of conventional tie hoops and crossties on the behavior of structural walls.

Figs. 2(c) and 2(d) show the reinforcement details of SFC180 and SFC90 where SFC was used selectively in the plastic hinge region. For SFC180 and SFC90, the longitudinal and horizontal

Table 1 Summary of test specimens

| Specimen | Spacing of boundary element transverse reinforcement | Concrete at plastic hinge zone |
|----------|--|--|
| RC180 | 180 mm | Plain concrete ($f'_c = 37.3$ MPa) |
| RC45 | 45 mm | Plain concrete ($f'_c = 37.3$ MPa) |
| SFC180 | 180 mm | 1.5% steel fiber concrete ($f'_c = 51.6$ MPa) |
| SFC90 | 90 mm | 1.5% steel fiber concrete ($f'_c = 51.6$ MPa) |

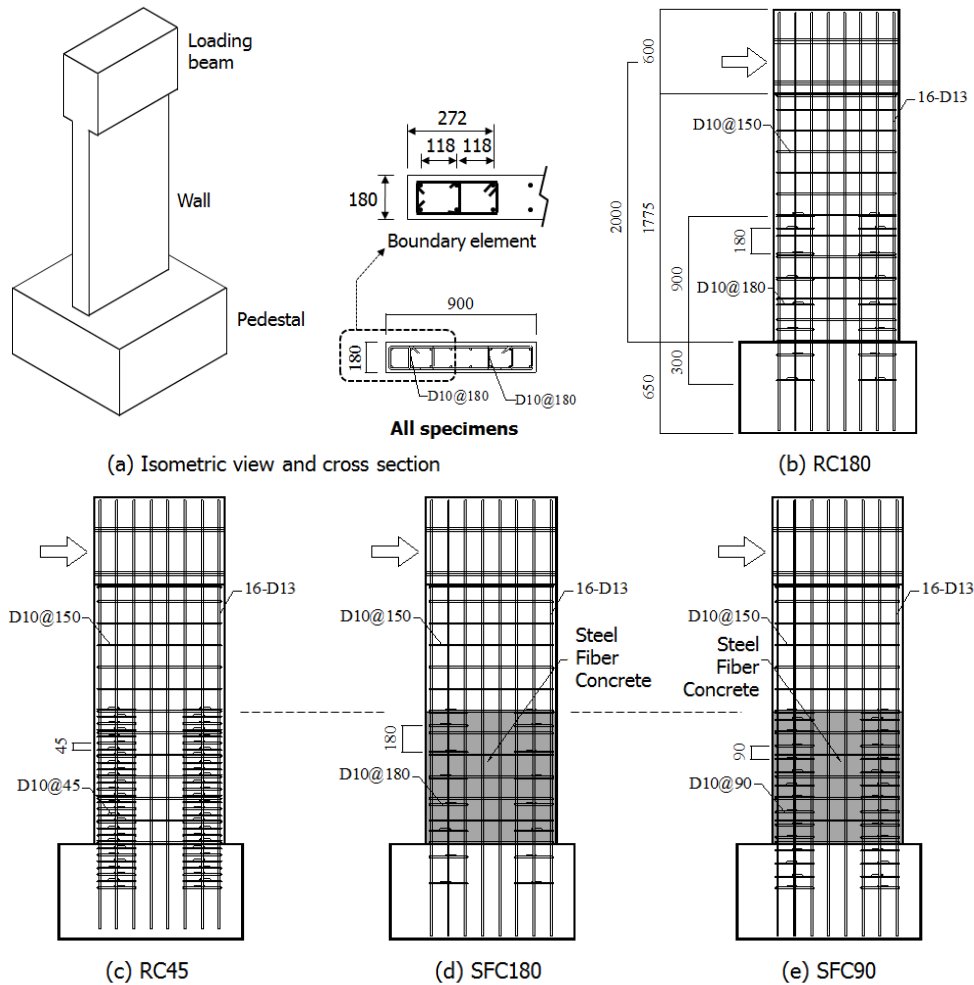


Fig. 2 Dimensions and reinforcement details of wall specimens

reinforcements were exactly the same as those of RC45. The depth of the boundary elements, $l_c = 272$ mm, was also the same that of RC45. However, the vertical spacing of the boundary element transverse reinforcement was intentionally increased to $s = 180$ mm ($= t$) for SFC180 and 90 mm ($= 0.5t$) for SFC90. Instead, SFC was used along with the conventional tie hoops and crossies. Thus the SFC was used to alleviate the strict confinement requirements of ACI 318 21.9.6. The SFC was used only in the plastic hinge region extending vertically from the base 900 mm; and plain concrete was used in the remaining parts including the pedestal and loading beam.

2.2 Materials

The compression test on concrete cylinders was performed at the test day (i.e. 40 days after the concrete casting). Though the design strength of concrete was 27MPa, the 40-day compressive strength of concrete was $f'_c = 37.3$ MPa on average. Table 2 shows the yield and tensile strengths

Table 2 Properties of reinforcing steel bars

| Bar type | Diameter | Area | Yield strength f_y | Tensile strength f_u | Yield ratio (f_u/f_y) |
|----------|----------|----------------------|----------------------|------------------------|---------------------------|
| D10 | 9.53 mm | 72.3 mm ² | 555 MPa | 675 MPa | 1.22 |
| D13 | 12.7 mm | 127 mm ² | 434 MPa | 568 MPa | 1.31 |

Table 3 Mix proportion of steel fiber concrete

| Concrete | | Steel fiber | | | | | | | | Slump (cm) | Air (%) |
|----------|---------|--------------------------------|-----|----|----|-----|-----|-----|----------------------|-------------|---------|
| W/C (%) | S/A (%) | Unit mass (kg/m ³) | | | | | | | Volume fraction (%) | | |
| | | W | C | SP | FA | S | G | AD* | | | |
| 46.2 | 47.0 | 172 | 261 | 74 | 37 | 797 | 913 | 2.6 | 0, 0.5, 1.0, and 1.5 | 20.5 ~ 21.5 | 2.1~3.0 |

* Super-plasticizer

of D10 and D13 steel reinforcing bars obtained from the direct tension tests. Despite the design yield strength was 400MPa, as shown in the table, the actual yield strength of D10 and D13 bars were $f_y = 555\text{MPa}$ and 434MPa on average, respectively. The ratios of tensile strength-to- yield strength ($=f_u/f_y$) were 1.22 for D10 bars and 1.31 for D13 bars.

For the SFC, end-hooked steel fibers were mixed with concrete (see Fig. 3(a)). The length and diameter of the steel fibers were 60 mm and 0.73 mm, respectively, and thus the aspect ratio was 82. The tensile strength of the steel fibers was 1220MPa. According to Nataraja *et al.* (1999), the behavior of the SFC depends on the volume fraction of steel fibers added to concrete. Thus, in order to investigate the best volume fraction of steel fibers securing higher deformation capacity and greater energy-absorbing capacity (or toughness), compression tests on the SFC cylinders (diameter = 100 mm and height = 200 mm) were previously conducted. Table 3 shows the mix proportioning of the SFC. As shown in Table 3, four volume fractions of 0.0, 0.5, 1.0, and 1.5 % were considered. The SFC cylinders were tested after 7-day steam curing. Fig. 3(b) shows the results of the compression test. The SFC with 1.5% steel fibers resulted in the highest ductility and the greatest toughness. Therefore, in this study, the SFC with 1.5% steel fibers was used for the wall specimens SFC180 and SFC90. Note that the compressive strength of the SFC at the test day, $f'_c = 51.6\text{MPa}$, was much greater than those of Fig. 3.

2.3 Test setup and loading protocol

Fig. 4 shows the test setup for the wall specimens. The wall specimens were subjected to a constant axial load $P_u = 729\text{kN}$ during cyclic loading. For the axial load, two vertically-installed actuators were used. For lateral loading, a horizontal actuator was attached to one end of the loading beam. The cyclic test was performed by controlling the lateral displacement of the specimens. Fig. 5 shows the loading history complying with ACI T1-1R (2001). The lateral displacement of each loading step was controlled to be within 125 ~ 150 % of the previous loading step. The load cycles were repeated three times at each loading step. An LVDT was used at the pedestal to measure possible slip.

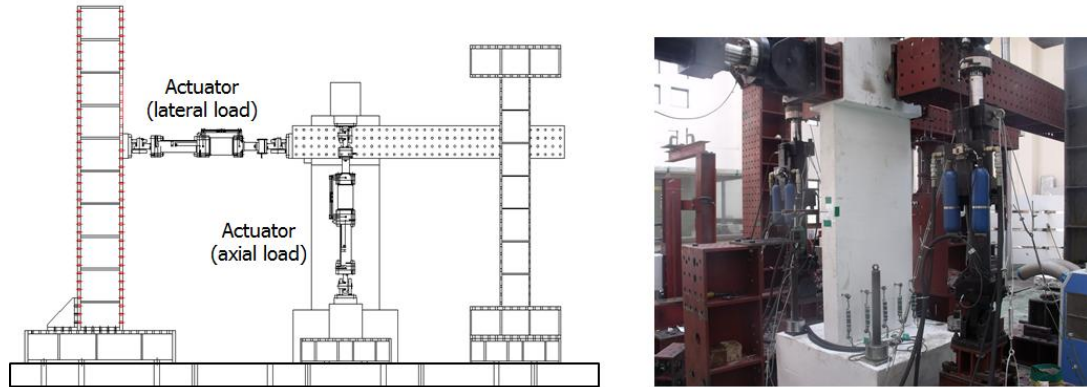


Fig. 4 Test setup

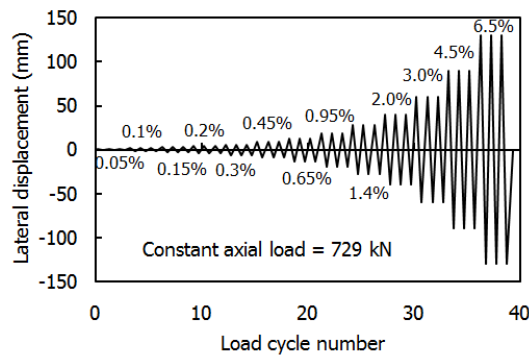


Fig. 5 Lateral loading history

3. Test results

3.1 Lateral load - drift ratio relationships and failure modes

Fig. 6 shows the lateral load-drift ratio relationships of the specimens. The drift ratio was defined as $\delta = \Delta/l_s$, where Δ = lateral displacement at the loading point and l_s = shear span length from the top of the pedestal to the loading point (= 2000 mm). Cracks and failure modes of the specimens at the end of the tests are shown in Fig. 7. For RC180 where the boundary elements were confined by conventional tie hoops and cross-ties at a spacing of 180 mm, as shown in Fig. 6(a), flexural yielding occurred at $\delta = 1.0\%$. Pinching due to the moderate axial load of $P_u = 729\text{kN}$ was observed during cyclic loading (Park and Eom 2006). As shown in Fig. 7(a), flexural cracking (or horizontal cracking) occurred first at the wall boundaries of the plastic hinge region. Then inclined shear cracking occurred in the web. As the lateral drift ratio and the number of repeated load cycles were increased further, the inclined shear cracks corresponding to positive and negative loadings intersected each other in the web. The spalling of cover concrete started at $\delta = 2.0\%$. During cyclic loading at $\delta = 3.0\%$, the crushing of concrete and the buckling of longitudinal D13 bars were observed in the boundary elements. Particularly, as the result of the spacing $s = 180$ mm of tie hoops and cross-ties greater than eight times the diameter of longitudinal

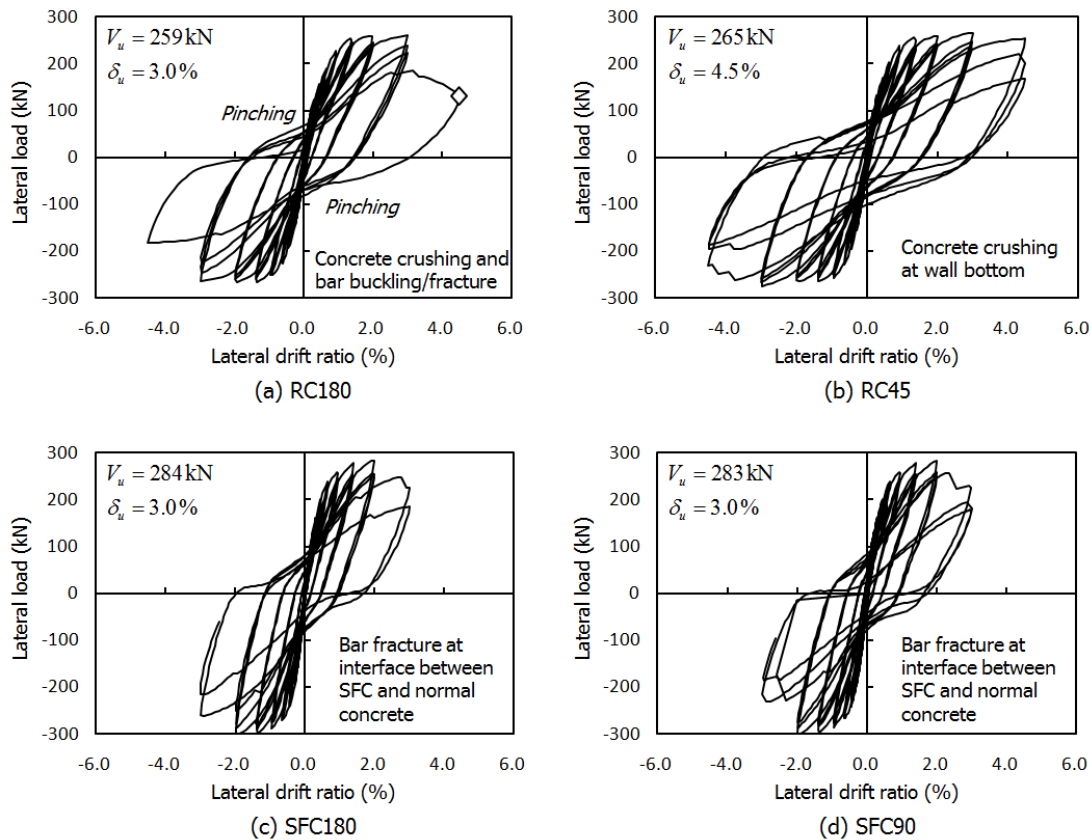


Fig. 6 Lateral load-drift ratio relationships

D13 bars ($= 8 \cdot 12.7 = 102$ mm), the bar buckling was premature and significant. Ultimately, RC180 lost the load-carrying capacity almost completely during the first cycle at $\delta = 4.5\%$ due to the crushing of concrete and the fracture of buckled D13 bars (see Fig. 7(a)).

For RC45 with the boundary elements confined by tie hoops and crossties at a spacing of 45 mm, as shown in Fig. 6(b), the overall cyclic behaviors including the load-carrying capacity, flexural yielding, pinching, and cracking pattern were similar to those of RC180. The spalling of cover concrete at the end did not occur until $\delta = 3.0\%$. At $\delta = 4.5\%$, the buckling of longitudinal D13 bars and the crushing of concrete in the boundary elements were observed. Ultimately, RC45 was failed during the third cycle at $\delta = 4.5\%$ due to the crushing of concrete and the fracture of buckled D13 bars (see Fig. 7(b)). The crushing of concrete and the buckling of D13 bars in RC45 were not as severe as in RC180 at the end of test as the result of the closely-spaced hoops and crossties ($s = 45$ mm). Thus the deformation capacity and hysteretic energy dissipation of RC45 were significantly improved.

Figs. 6(c) ~ (d) and Figs. 7(c) ~ (d) show the test results of SFC180 and SFC90. The overall cyclic behaviors of SFC180 and SFC90 were similar to that of RC180. However, due to the tensile resistance of the SFC, the initial stiffness and peak strength of SFC180 and SFC90 were slightly increased. Furthermore, flexural and shear cracks in the plastic hinge regions were

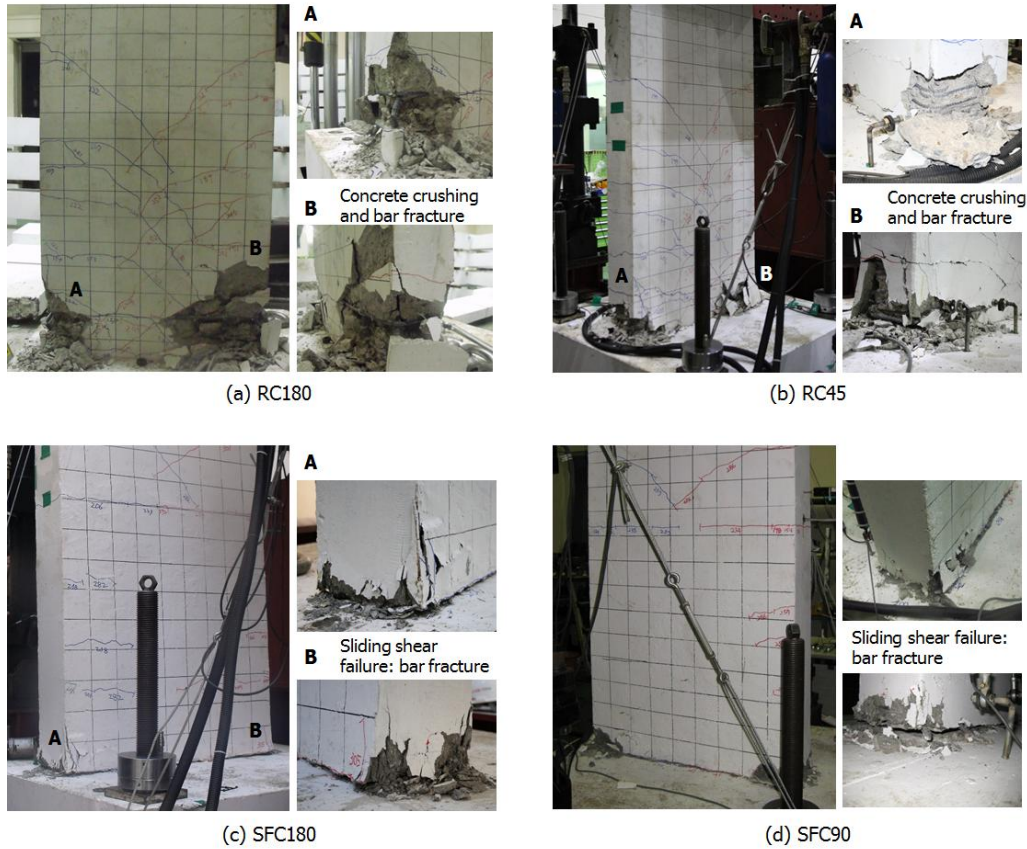


Fig. 7 Crack patterns and failure modes

significantly reduced when compared to those of RC180 and RC45. The spalling and crushing of concrete at the bottom end were significantly alleviated even at the end of test, as shown in Figs. 7(c) ~ (d). These indicate that plastic deformation was not significant in the potential plastic hinge region (i.e. in the region of 900 mm high from the wall bottom). Instead, both SFC180 and SFC90 where the SFC was used exclusively in the plastic hinge region suffered sliding shear failure at the interface of the SFC and plain concrete (i.e. the wall-pedestal interface) at a moderate drift ratio of 3.0%. Ultimately, the longitudinal D13 bars were fractured due to the sliding shear. The sliding shear failure of SFC180 and SFC90 was discussed in more detail in chapter 3.3.

3.2 Strength, stiffness, ductility, and energy dissipation

Fig. 8 shows the envelop curves of the wall specimens. Table 4 shows the peak strength V_u , yield drift ratio δ_y , maximum drift ratio δ_u , displacement ductility μ , and yield stiffness K_y defined from the envelope curves. δ_u was defined as the drift ratio when the load-carrying capacity was decreased to $0.75V_u$. K_y was determined as the secant stiffness passing through the point of $0.75V_u$ on the pre-peak envelope curve (see Fig. 8). Then δ_y was calculated by dividing V_u by K_y . The displacement ductility was calculated by dividing δ_u by δ_y : $\mu = \delta_u/\delta_y$.

For RC180 and RC45, the V_u values were almost same because the amount and arrangement of longitudinal D13 bars were identical (see Table 4). The K_y values were also equivalent. However, $\delta_u = 4.5\%$ ($\mu = 5.42$) of RC45 with the smaller spacing of tie hoops and crossties ($s = 45$ mm) was greater than $\delta_u = 3.0\%$ ($\mu = 3.15$) of RC180 with the greater spacing ($s = 180$ mm). For SFC180 and SFC90, the K_y values and V_u values were greater than those of RC180 and RC45. The δ_u values of SFC180 and SFC90 were the same as that of RC180. However, the μ values of SFC180 and SFC90 were slightly increased due to the less δ_y . Note that, for SFC180 and SFC90, the strict confinement requirements for the boundary elements of ACI 318 21.9.6 were intentionally alleviated by using the SFC. Thus the purpose of this study was to investigate the behavior of the boundary elements confined by the SFC and then to verify the deformation capacity of SFC180 and SFC90 through the test. However, such purpose was not appropriately verified yet due to the unexpected sliding shear failure at the wall base (see Table 4).

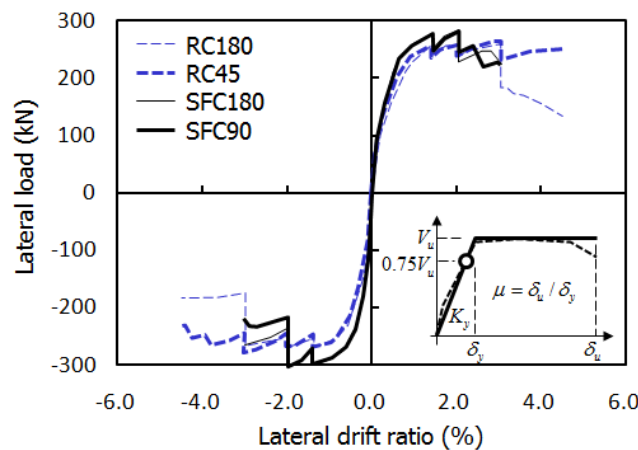


Fig. 8 Envelope curves

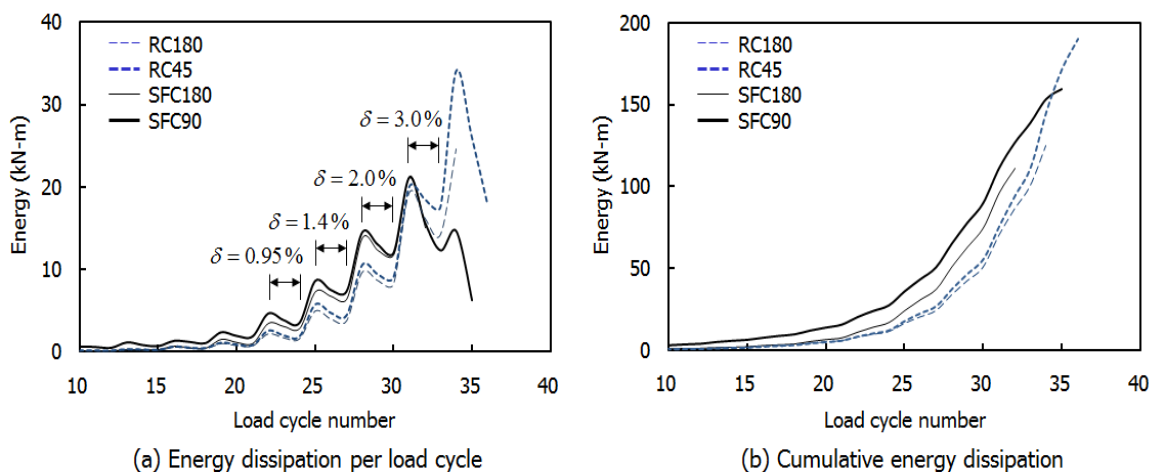


Fig. 9 Hysteretic energy dissipation

Table 4 Test results

| Specimen | Yield drift ratio δ_y (%) | Max. drift ratio δ_u (%) | Ductility $\mu (= \delta_u / \delta_y)$ | Peak strength V_u (kN) | Yield stiffness K_y (kN·mm/mm) | Failure mode |
|----------|----------------------------------|---------------------------------|---|--------------------------|----------------------------------|---------------------|
| RC180 | 0.95 | 3.0 | 3.15 | 259 | 273 | Flexure-compression |
| RC45 | 0.83 | 4.5 | 5.42 | 265 | 319 | Flexure-compression |
| SFC180 | 0.70 | 3.0 | 4.29 | 284 | 406 | Sliding shear |
| SFC90 | 0.69 | 3.0 | 4.34 | 283 | 410 | Sliding shear |

Fig. 9 compares the hysteretic energy dissipation of the specimens. As shown in Fig. 9(a), the energy dissipations per load cycle of SFC180 and SFC90 were greater than those of RC180 and RC45 until the 30th load cycle because the peak strengths of SFC180 and SFC90 were slightly greater than those of RC180 and RC45 (see Fig. 8 and Table 4). The steel fibers might hardly contribute to the energy dissipation per load cycle because the plastic hinge regions of SFC180 and SFC90 remained elastic (see Figs. 7(c) and 7(d)). Fig. 9(b) compares the cumulative energy dissipation of the specimens. SFC180 and SFC90 dissipated greater energy initially. However, ultimately RC45 with the greatest ductility showed the greatest cumulative energy dissipation.

3.3 Sliding shear failure of SFC180 and SFC90

For cantilever walls, the flexural demand is the highest in the wall base as the gradient of bending moment is triangular. Therefore, flexural yielding starts in the wall base and then propagates into the plastic hinge region, as shown in the test results of RC180 and RC45. For SFC180 and SFC90 where the SFC with high tensile strength was used exclusively in the plastic hinge region, however, the tensile strength of SFC prevents the flexural yielding at the wall base from spreading over the plastic hinge region. Thus plastic deformation concentrates on the vicinity of the wall base. This increases an anchorage slip of longitudinal bars at the wall base (Tastani and Pantazopoulou 2013), alleviating the strains of concrete and longitudinal bars in the plastic hinge region. Of course, concrete cracking is significantly reduced in SFC180 and SFC90 as the result of the alleviated strains of concrete (see Fig. 7(c) and 7(d)). However, the increased anchorage slip at the wall base causes the sliding shear failure as well by growing a gap at the interface of dissimilar materials (Paulay and Priestley 1992, see Fig. 10).

The gap-growing in SFC180 and SFC90 can be demonstrated from the measurement. Fig. 11 shows the locations of five LVDTs with a spacing of 200 mm installed at a height of 450 mm from the wall base. The vertical strains over the wall cross section in the plastic hinge region were calculated by dividing the LVDT deformations (elongation and shortening) by 450 mm. Figs. 11(a) and (b) show the strain distributions of RC45 and SFC90. Since the strain distributions of RC180 and SFC180 were very similar to those of RC45 and SFC90, respectively, only the test results of RC45 and SFC90 were presented here. The strain distributions of Fig. 11 were the measurements at $\delta = 0.65\%$ (1st cycle), 2.0% (1st and 3rd cycles), and 3.0% (1st cycle). The strains at $\delta = 0.65\%$ where the walls began to yield in flexure were marked as dash-dot lines. The strains at $\delta = 2.0\%$ and 3.0% were marked as the dotted and solid lines, respectively. For RC45, one end was tensile strain while the other end was compressive strain. Thus the concrete of the compression zone substantially resisted the wall shear. For SFC90, however, tensile strains were

developed over the entire cross section. Furthermore, during the 1st and 3rd load cycles at $\delta = 2.0\%$, the tensile strains were increased (compare the thick and thin dotted lines in Fig. 11(b)). This indicates that a gap or horizontal crack penetrated through the overall wall depth at the interface.

Once the gap or horizontal crack is completely open over the cross section, the sliding shear at the interface should be resisted by the dowel action of longitudinal bars, as illustrated in Fig. 10(b). For this reason, the longitudinal bars of SFC180 and SFC90 suffered significant slip and were ultimately fractured, as shown in Figs. 7(c) and 7(d). Such sliding shear failure is not favorable because brittle failure due to premature bar fracture can occur. Thus, when the SFC is used selectively for high stress zone, strain concentration at the interface of dissimilar materials should be addressed. To protect the unexpected early sliding failure, this interface should be avoided by curing the SFC into wall and pedestal together. The use of the shear connector in this interface can also be considered to protect this unexpected sliding failure.

4. Section analysis

4.1 Stress-strain relationship of confined concrete and SFC

For the concrete confined by conventional tie hoops and crossies, the stress-strain relationship proposed by Mander *et al.* (1988) was used.

$$\sigma_c = f'_{cc} \left(\frac{(\epsilon_c / \epsilon_{cc})^r}{r - 1 + (\epsilon_c / \epsilon_{cc})^r} \right) \text{ for } \epsilon_c \leq \epsilon_{cu} \tag{1}$$

where σ_c and ϵ_c = compressive stress and strain, respectively, of the confined concrete; f'_{cc} = compressive strength of the confined concrete; ϵ_{cc} = compressive strain at f'_{cc} ($= \epsilon_{co}[1+5(f'_{cc}/f'_c-1)]$); ϵ_{co} = compressive strain at f'_c ($= 0.002+0.001(f'_c-20)/80$), Foster and Gilbert 1996); $r = E_c/(E_c - f'_{cc}/\epsilon_{cc})$; $E_c = 5000\sqrt{f'_c}$ (MPa); and ϵ_{cu} = ultimate compressive strain of the confined concrete. The tensile stress of the confined concrete was ignored.

Fig. 12(a) shows the stress-strain relationship of the SFC. As the volume fraction of steel fibers increases, ϵ_{co} at f'_c increases and the slope of the descending portion is less steep than that of plain concrete. In the present study, the stress-strain relationship of SFC under compression is defined as the parabolic-linear curve as follows.

$$\sigma_c = f'_c \left[2 \left(\frac{\epsilon_c}{\epsilon_{co}} \right) - \left(\frac{\epsilon_c}{\epsilon_{co}} \right)^2 \right] \text{ for } \epsilon_c \leq \epsilon_{co} \tag{2a}$$

$$\sigma_c = f'_c - \left(\frac{\epsilon_c / \epsilon_{co} - 1}{\epsilon_{cu} / \epsilon_{co} - 1} \right) (f'_c - \sigma_r) \text{ for } \epsilon_{co} < \epsilon_c \leq \epsilon_{cu} \tag{2b}$$

where σ_r = residual stress at ϵ_{cu} . In Eq. (2) and Fig. 12(a), the ascending and descending portions were idealized as the parabolic and linear relationships, respectively. Fig. 12(b) compares the stress-strain relationships of the plain concrete and SFC with the volume fractions of 0.5%, 1.0%, and 1.5% shown in Fig. 3(b) with the proposed σ_c - ϵ_c relationships. The values of f'_c , ϵ_{co} , ϵ_{cu} , and σ_r of the plain concrete and SFC obtained from the compression tests are also presented in the figure. For the SFC with the volume fractions of 1.0% and 1.5%, the σ_c - ϵ_c relationships were drawn until $\epsilon_{cu} = 0.02$. As shown in Fig. 12(b), the proposed σ_c - ϵ_c relationships correlated well

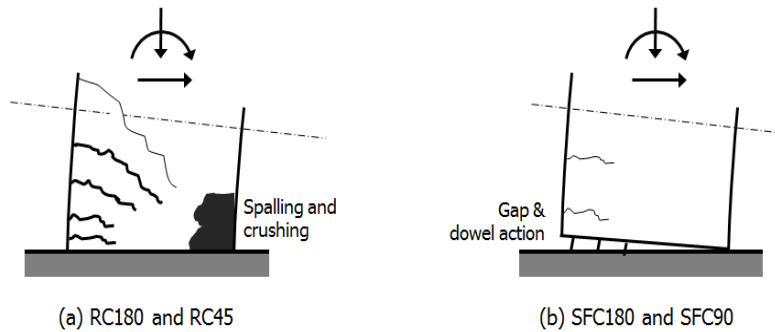


Fig. 10 Flexure-compression failure vs. sliding shear failure

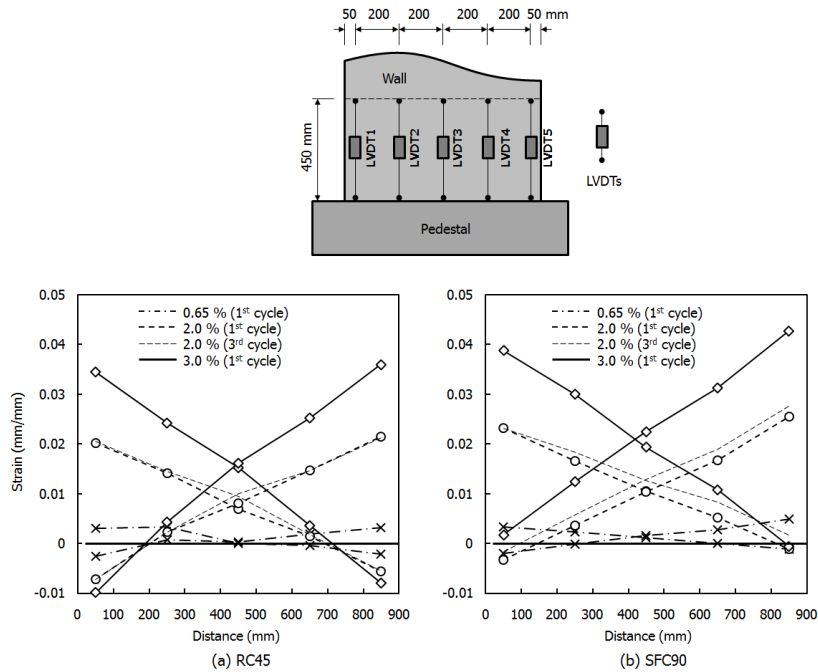


Fig. 11 Strains measured from LVDTs in plastic hinge region

with the results of the compression tests. Although Nataraja *et al.* (1999) suggested an elaborate relationship addressing the change of volume fraction of steel fibers, the present study used the simplest relationship which is popular with practice engineers.

For SFC under tension, the $\sigma_c - \varepsilon_c$ relationship is defined based on ACI Committee 544 (1988) as follows (see Fig. 12(a)).

$$\sigma_c = \bar{E}_c \varepsilon_c \leq -\sigma_t \quad \text{for } \varepsilon_c < 0 \tag{3}$$

where $\bar{E}_c = 2f_c'/\varepsilon_{co}$; σ_t = ultimate tensile strength ($= 0.00772[l_f/d_f]\rho_f F_{be}$, ACI Committee 544 1988); l_f and d_f = length and diameter of steel fiber, respectively; ρ_f = volume fraction of steel fibers in percentage; and F_{be} = bond efficiency of steel fiber varying from 1.0 to 1.2. In Eq. (3), the tensile stress and strain are negative values.

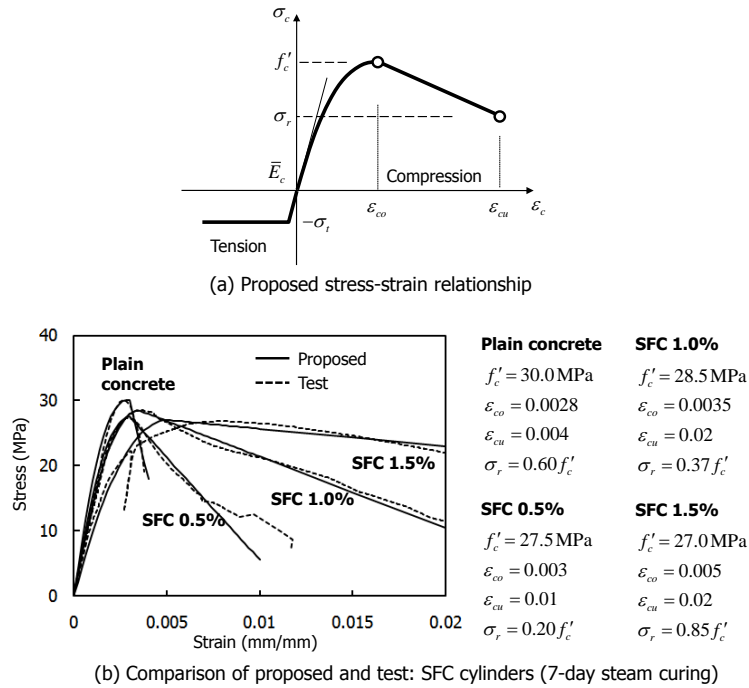


Fig. 12 Stress-strain relationship of SFC varying with volume fraction of steel fibers

4.2 Results of wall section analysis

Numerical section analysis was performed to investigate the effect of the confined concrete and SFC on the deformation capacity of wall specimens. For RC180, the confinement effect of the tie hoops and crossties provided for the boundary elements at a spacing of 180 mm is negligible. Thus the σ_c - ϵ_c relationship of concrete corresponding to $f'_c = 37.3$ MPa, $\epsilon_{co} = 0.00222$, $\epsilon_{cu} = 0.004$, and $\sigma_r = 0.6f'_c$ was used for the section analysis of RC180 (refer to Eqs. (2a) and (2b)). The σ_c - ϵ_c relationship of concrete is the same as that of the plain concrete in Fig. 12(b), except that the concrete strength was increased from 30.0MPa to $f'_c = 37.3$ MPa. On the other hand, for RC45 with the boundary elements confined by the tie hoops and crossties at a spacing of 45 mm, the compressive strength and ultimate strain of the confined concrete were calculated as $f'_{cc} = 70.3$ MPa, $\epsilon_{cc} = 0.0120$, and $\epsilon_{cu} = 0.065$ (Mander *et al.* 1988). For unconfined concrete, the same σ_c - ϵ_c relationship as that used for RC180 was used. For the section analysis, the layer approach based on linear strain distribution over the cross section was used. During the analysis, the unconfined concrete and confined concrete were separately addressed. The axial load on the cross section (= 729kN) was kept constant throughout the analysis.

Fig. 13 shows the moment-curvature relationships of RC180 and RC45. The thick solid and dashed lines indicate RC45 and RC180, respectively. For comparison, the moment-curvature relationship of RC45 measured from the test is also presented as grey dotted lines in Fig. 13(a). The moments were calculated by multiplying the lateral loads by the shear span $l_s = 2000$ mm. The curvatures were calculated by using the vertical displacements of LVDT1 and LVDT5, Δ_1 and Δ_5 ,

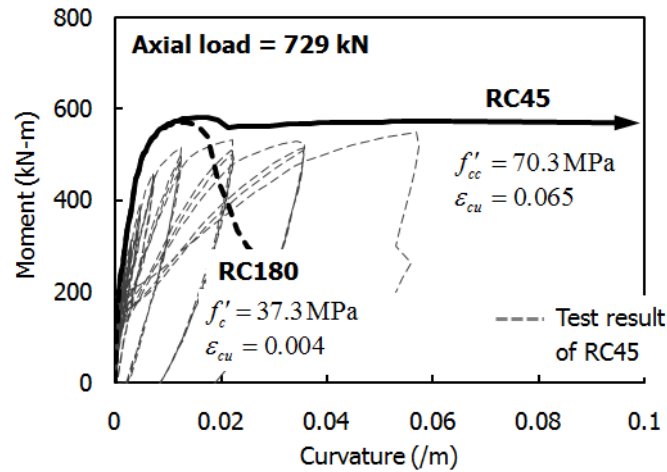


Fig. 13 Predicted moment-curvature relationships of RC180 and RC45

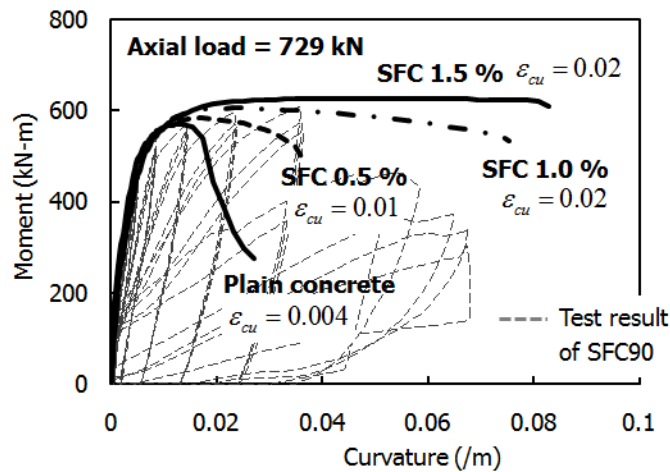


Fig. 14 Predicted moment-curvature relationships of walls with SFC

respectively: $\phi = (\Delta_1 - \Delta_5)/(450 \cdot 800)$, where 450 mm and 800 mm of the denominator are the gage length and horizontal distance of the LVDTs, respectively (see Fig. 11). As shown in Fig. 13, the peak strengths of RC45 and RC180 were equivalent, despite the increased compressive strength $f'_{cc} = 70.3 \text{ MPa}$ of the confined concrete. However, the predicted deformation capacities of RC180 and RC45 were clearly contrasted. As the result of increased deformation capacity of the confined concrete (i.e. $\varepsilon_{cu} = 0.065$), RC45 showed a ductile behavior retaining its load-carrying capacity until $\phi = 0.1 / \text{m}$. On the other than, for RC180, the load-carrying capacity was degraded early at $\phi = 0.02 / \text{m}$ due to the crushing of the unconfined concrete at $\varepsilon_{cu} = 0.004$. Note that the predicted deformation capacity of RC45 was far greater than the test result. This might be because the ultimate strain $\varepsilon_{cu} = 0.065$ of the confined concrete used in the analysis was greater than the actual failure strain. As shown in Fig. 11(a), the peak compressive strain of concrete measured over a distance of 450 mm was about 0.01.

For the section analysis of SFC180 and SFC90, the stress-strain relationship of the SFC under compression was constructed with the values of $f'_c = 51.6\text{MPa}$, $\varepsilon_{co} = 0.005$, $\varepsilon_{cu} = 0.02$, and $\sigma_r = 0.85 f'_c$. The properties were the same as those of the SFC 1.5% shown in Fig. 12(b), except for $f'_c = 51.6\text{MPa}$. The tensile strength of the SFC was $\sigma_t = 1.14\text{MPa}$ ($\rho_f = 1.5\%$, $l_f = 60\text{ mm}$, $d_f = 0.73\text{ mm}$, and $F_{be} = 1.2$, see Eq. (3)). To investigate the wall behavior depending on the volume fraction of the SFC, the section analysis was performed for the SFC 0.5% ($f'_c = 51.6\text{MPa}$, $\varepsilon_{co} = 0.003$, $\varepsilon_{cu} = 0.01$, and $\sigma_r = 0.2 f'_c$) and SFC 1.0% ($f'_c = 51.6\text{MPa}$, $\varepsilon_{co} = 0.0035$, $\varepsilon_{cu} = 0.02$, and $\sigma_r = 0.85 f'_c$) as well. Note that the values of ε_{co} , ε_{cu} , and σ_r defining the descending behavior of the stress-strain relationships of the SFC under compression significantly varied with the volume fraction ρ_f , while the compressive strength $f'_{cc} = 51.6\text{MPa}$ was same.

Fig. 14 shows the moment-curvature relationships for the plain concrete, SFC 0.5%, SFC 1.0%, and SFC 1.5%. For comparison, the test result of SFC90 is also presented in the same figure. The ductility and the post-peak behavior of the cross sections were significantly improved as the volume fraction of steel fibers was increased from 0.0% to 1.5%. This indicates that the slope of the post-peak descending behavior of the SFC under compression significantly affected the overall ductility of the walls though it barely affects the peak strengths of walls. The moment capacity of the cross sections was slightly increased due to the tensile strength σ_t of SFC as the volume fraction of steel fibers increases. Note that the results of the section analysis should not be directly compared with the test result because the failure mode of SFC90 was the sliding shear failure, rather than the flexure-compression failure. In this study, section analysis was performed to investigate the moment-curvature relationship of only the lower part of wall specimens. Therefore, for the section analysis, it was assumed that the flexural failure occurred by avoiding the sliding failure at the interface.

5. Summary and Conclusions

In the present study, the seismic behavior of structural walls with the boundary elements confined by conventional tie hoops and SFC was investigated. From the cyclic load tests on four wall specimens, the load-carrying capacity, ductility, energy dissipation, and failure mode were evaluated. An increase in the deformation capacity was observed in the specimen complying with the confinement requirements of ACI 318-11 21.9.6. For the specimens where SFC was used exclusively in the plastic hinge region, the cracking and spalling of concrete were substantially reduced and the strength, energy dissipation capacity, and yield stiffness were enhanced. However, the specimens were failed due to the sliding shear at the interface between SFC and plain concrete, rather than flexure-compression failure, and as a result the deformation capacity was not increased. The effects of conventional tie hoops (including cross-ties) and SFC were also investigated through the nonlinear section analysis based on the stress-strain relationships of the confined concrete and SFC. The results showed that the ductility of walls can be significantly affected by the post-peak descending behavior of the SFC depending on the volume fraction of steel fibers.

In general, the descending behavior of SFC is ignored in the calculation of strength. ACI 544.4R (1988) recommends the flexural strength of reinforced concrete members with steel fibers be calculated for the compressive stress at $\varepsilon_{cu} = 0.003$ and constant tensile strength σ_t . As shown in Fig. 14, the flexural strength of ACI544.4R is reasonable for strength design. However, in seismic design, the post-peak descending behavior of SFC also needs to be addressed because it can

improve the ductility of the member, although the following aspects should be considered further.

- The ductility of walls depends on the volume fraction of steel fibers (see Fig. 14). Therefore, the volume fraction of steel fibers should be carefully controlled to secure the smooth post-peak descending behavior of SFC with high ductility and toughness. The parametric study of the present study suggests that the volume fraction of 1.0~ 1.5% steel fibers might be favorable.
- If SFC is selectively used along with plain concrete in a member or structure, attention should be paid to the interface shear between the SFC and plain concrete. The tensile strength σ_t of SFC can increase the flexural and shear strengths of the member. This can potentially change the failure mode and thus plastic damage may be concentrated on the relatively weak interface (refer to the sliding shear failure shown in Fig.7(c) and 7(d)).

Acknowledgments

This research was supported by Daelim Industrial Co. and by Basic Science Research Program through the National Research Foundation of Korea (NRF) funded by the Ministry of Education, Science, and Technology (2011-0003288 and 2012R1A1A1003282).

References

- ACI Committee 544 (1988), "Design considerations for steel fiber reinforced concrete", *ACI Struct. J.*, **95**(5), 563-580.
- American Concrete Institute (2001), Commentary on acceptance criteria for moment frames based on structural testing (ACI T1.1R-01), Farmington Hills, Michigan.
- Andre, F., Sylvain, P. and Jules, H. (1995), "Seismic Behavior of Steel-Fiber Reinforced Concrete Interior Beam-Column Joints", *ACI Struct. J.*, **92**(5), 543-552.
- American Concrete Institute (2011), *Building Code Requirements for Structural Concrete*, ACI 318-11 and ACI 318R-11, Farmington Hills, Michigan.
- Chaallal, O., Thibodeau, S., Lescelleur, J. and Malenfant, P. (1996), "Steel fiber or conventional reinforcement for concrete shear wall", *Concrete Int.*, **18**(6), 39-42.
- Craig, R.J., McConnell, J., Germann, H., Dib, N. and Kashani, F. (2005), "Behaviors of reinforced fibrous concrete columns", *ACI Special Publication*, SP81-4, 69-105.
- Filiatrault, A., Ladicani, K. and Massicotte, B. (1994), "Seismic performance of code-designed fiber reinforced concrete joints", *ACI Struct. J.*, **91**(5), 564-571.
- Foster, S.J. and Gilbert, R.I. (1996), "The design of non-flexural members with normal and high-strength concrete", *ACI Struct. J.*, **93**(1), 3-10.
- Henager, C.H. (1977), "Steel fibrous ductile concrete joint for seismic-resistant structures", *ACI Special Publication: Reinforced Concrete Structures in Seismic Zones*, SP-53, American Concrete Institute, Detroit, 371-386.
- Jiuru, T., Chaobin, H., Kaijian, Y. and Yongcheng, Y. (1992), "Seismic behavior and shear strength of framed joint using steel-fiber reinforced concrete", *J. Struct. Eng., ASCE*, **118**(2), 341-358.
- Mander, J.B., Priestley, M.J.N. and Park, R. (1988), "Theoretical stress-strain model for confined concrete", *J. Struct. Eng., ASCE*, **114**(8), 1804-1826.
- Nataraja1, M.C., Dhang, N. and Gupta, A.P. (1999), "Stress-strain curves for steel-fiber reinforced concrete under compression", *Cement Concrete Compos.*, **21**(5-6), 383-390
- Park, H. and Eom, T. (2006), "A simplified method for estimating the amount of energy dissipated by flexure-dominated reinforced concrete members for moderate cyclic deformations", *Earthq. Spectra*,

- 22(2), 459-490.
- Park, H., Kang, S., Chung, L. and Lee, D. (2007), "Moment–curvature relationship of flexure-dominated walls with partially Confined End-Zones", *Eng. Struct.*, **29**(1), 33-45.
- Paulay, T. and Priestley, M.J.N. (1992), *Seismic Design of Reinforced Concrete and Masonry Buildings*, John Wiley and Sons Inc., New York.
- Sullivan, T.J. (2010), "Capacity design considerations for RC frame-wall structures", *Earthq. Struct.*, **1**(4), 391-410.
- Tastani, S.P. and Pantazopoulou, S.J. (2013), "Yield penetration in seismically loaded anchorages: effects on member deformation capacity", *Earthq.Struct.*, **5**(5), 527-552.
- Thomsen, J.H. and Wallace, J.W. (1995), *Displacement-Based Design of RC Structural Wall: An Experimental Investigation of Walls with Rectangular and T-shaped Cross-Sections*, Report No. Cu/Cee-95-06, Department of civil and environmental Engineering at Clark University.
- Wallace, J.W. (1994), "A new methodology for seismic design of reinforced concrete shear walls", *J. Struct. Eng., ASCE*, **120**(3), 863-884.
- Wallace, J.W. (1995), "Seismic design of RC structural walls. Part I: New code format", *J. Struct. Eng., ASCE*, **121**(1), 75-87.
- Wallace, J.W. and Moehle, J.P. (1992), "Ductility and detailing requirements of bearing wall buildings", *J. Struct. Eng., ASCE*, **118**(6), 1625-1644.
- Wallace, J.W. and Orakcal, K. (2002), "ACI 318-99 Provisions for Seismic Design of Structural Walls", *ACI Struct. J.*, **99**(4), 499-508.